April 2017

Gold - Human Serum Albumin Contrast Agents

Sarah K. Fields
Worcester Polytechnic Institute

Gold - Human Serum Albumin Contrast Agents

A Major Qualifying Project
Submitted to the faculty of
Worcester Polytechnic Institute
in partial fulfillment of the requirements
for the Degree of Bachelor of Science

Written By:
Sarah Fields

Project Advisor:
Professor Drew Brodeur

Project Sponsor:
Dr. Gang Han
University of Massachusetts Medical School

May 2017

Abstract

Traditional contrast agents use inorganic compounds containing metal ions to differentiate tissue types in medical diagnostic imaging. These compounds suffer from toxicity and they do not target specific tissues. A human serum albumin and gold complex (Au@HSA) was synthesized via a biomineralization reaction to overcome these obstacles and the resulting compound was optically active, giving it potential as a contrast agent. Additionally, the Au@HSA was conjugated with the tumor targeting compound arginylglycylaspartic acid without losing its optical activity.

Acknowledgments

This project would not have been possible without the sponsorship of University of Massachusetts Medical School. All research was completed at their lab under the direction and supervision of Dr. Gang Han. This research was a continuation of the research by Dr. Yang Zhao who also lended his expertise on the subject throughout the project.

I would also like to thank Professor Drew Brodeur as the on-campus advisor. This project was possible because of his guidance and support.

Table of Contents

Table of Figures

Table of Tables

1. Introduction

Since the discovery of magnetic resonance imaging (MRI), it has become a useful diagnostic tool in medicine. MRI can be used to find abnormalities in different tissues including: the body, brain, and heart. Contrast agents (CA) can be used to enhance MRI images and make it easier to differentiate between tissue types. The most common CAs are gadolinium (Gd) based compounds. The FDA has approved nine Gd CAs including gadoterate meglumine (Dotarem), gadabutrol (Gadavist), and gadodiamide (Omniscan). However, the FDA also has safety concerns about these CAs; they are currently looking into the accumulation of Gd in the brain of patients who have had multiple MRIs (U.S. Food and Drug Administration 2016-b). Other downsides to Gd based CAs include not targeting any specific tissue types-such as a tumor-and short *in vivo* half-lives, leading to a brief window of time for the scan to take place. The traditional Gd CAs are difficult to synthesize in the lab as well.

Near-infrared fluorescence imaging (NIRFI) is another type of imaging that is starting to become more common. The discovery of new CAs has increased the diagnostic properties of NIR imaging for visualizing different tissue types. Currently there are only three FDA approved contrast agents: indocyan green, methylene blue, and fluorescein (Garland 2016). None of these contrast agents are specifically tumor targeting compounds.

This research introduces a gold and human serum albumin complex (Au@HSA) easily synthesized via a biomineralization reaction that can be used in MRI and NIRFI. The complex's tumor targeting ability was increased by conjugation with arginylglycylaspartic acid (RGD).

2. Background

2.1 Magnetic Resonance Imaging

2.1.1 Uses of Magnetic Resonance Imaging

MRI is used to take high definition images of the human body to aid in medical diagnosis. When MRI was discovered in 1946, it created an image of a thin slice of the body, but through advancements of MRI and the use of computers, a three dimensional image can now be formed. In 1971, the difference in signal for tissue and tumors was noticed, thus suggesting that MRI could be used for medical diagnoses (Hornak 2011-c).

Today, MRI of the body can be used to find abnormalities of the tissue, such as tumors in organs. It can also show irregularities in the brain and spinal cord. Within the brain, a functional MRI can also show activity levels in different regions of the brain. MRI can be used to examine the structure of the heart as well as the flow of blood through vessels and arteries. Another use for MRI is to look at the chemical composition of tissue (U.S. Food and Drug Administration 2016-b).

2.1.2 Mechanism of Magnetic Resonance Imaging

MRI is based on nuclear magnetic resonance (NMR) and shares many of the same mechanisms. Both methods monitor changes in a magnetic field by measuring the spin of the hydrogens atoms in the body's water and fat stores; the human body comprises about 63% hydrogen atoms. (Hornak 2011-d).

Unpaired electrons, protons and neutrons each have a spin value that can be either positive ½ or negative ½. This ½ spin will create a small magnetic field which causes a disturbance in the magnetic field generated by the MRI scanner. Every subatomic particle has an equilibrium spin state with a net magnetization. When the system is exposed to the frequency of

energy that is equal to the difference in energy between the spin states, the net magnetization is changed (Hornak 2011-b). The conventional system is to place the net magnetization and external magnetic field along the z-axis of an x,y,z coordinate system. Longitudinal relaxivity (T_1) refers to the length of time required to return the z-component of the net magnetization to return to equilibrium (Reich et al. 2016).

2.1.3 Magnetic Resonance Imaging Contrast Agents

To transform the MRI scan information into a useful image, the tissue types have to be differentiated. MRI CAs change the signal intensity between different tissue types, allowing for clearer images. The contrast agent can be used to target a specific tissue type, for instance a tumor, making it easier to visualize the tissue type (Hornak 2011-c).

Paramagnetic CAs can interact with the net magnetization of the subatomic particles. The disturbance can lengthen the time required for the net magnetization to return to equilibrium. This means T_1 increases in water, thus changing the signal intensity. The paramagnetic CA is able to vary the magnetic field because unpaired electrons can change their spin. The change in the magnetic field will change T_1 based on the formula:

$$1/T_{1\,(Measured)} = 1/T_{1\,(Water)} + r_1\,[A]$$

The change in T_1 is dependent on the relaxivity (r_1) and the concentration of the paramagnetic material, [A] (Hornak 2011-a). Common paramagnetic ions are manganese (Mn^{+2}), iron (Fe^{+3}), or gadolinium (Gd^{+3}); these ions have multiple unpaired electrons. Gd^{3+} is the most common paramagnetic CA because of its 7 unpaired electrons (Pirollo et al. 2006). Gold nanoclusters have also been shown to be MRI CAs, especially when complexed with proteins (Chen et al. 2015).

There are three main types of CAs: intravascular, extracellular, and intracellular. Intravascular CAs stay in the vascular system and can be used for monitoring blood flow. Extracellular CAs travel into the extracellular fluid without entering the cells. Since tumors often have a more extensive network of extracellular fluid than other tissue types, these CAs have a higher concentration in the tumor cells and produce a stronger signal intensity. Intracellular CAs enter the cell; they can be designed to target a specific type of cell (Hornak 2011-a).

2.2 Near Infrared Fluorescence Imaging

NIRFI uses wavelengths in the near infrared region (NIR) (700-1000 nm) to produce fluorescence that is then recorded to create images of the body. Water, melanin, proteins and hemoglobin, which are the main constituents of human flesh, absorb in the 200 to 650 nm range (Figure 1). This means that using visible light causes all human tissue to fluoresce and is not useful in visualizing specific tissue (Pansare et al. 2012). The NIR wavelengths do not cause the tissue to fluoresce so that CAs can clearly be seen.

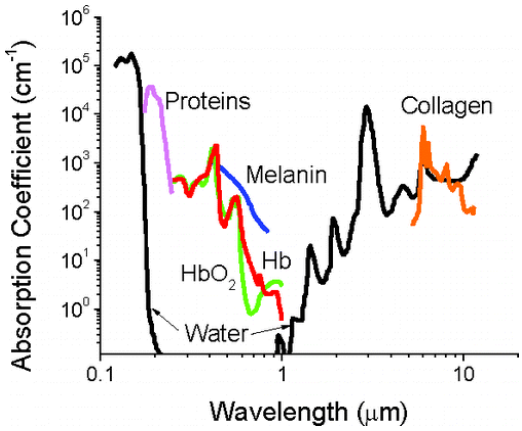

Figure 1: The absorption wavelengths of different tissue components (Pansare 2012)

To visualize tissue, contrast agents that target specific tissue or cell types are used. Researchers have been working on CAs to perform vascular mapping of the eye, brain, breast,

brown adipose tissue and the heart. Experimental CAs can also show inflammation, atherosclerosis, protease activity, cell death, and tumor tissue (Frangioni 2003).

2.3 Gold Nanoclusters

2.3.1 Properties

Gold nanoclusters (AuNCs) generally have a diameter of less than 1 nm and comprise a few to tens of gold atoms (Xie et al. 2009). The AuNCs exhibit fluorescence due to their unpaired electron. This fluorescence can be controlled from the visible to the near-infrared range by adjusting the size of the nanocluster or conjugating with other molecules (Shang & Nienhaus 2012). AuNCs can be synthesized using a variety of methods including the use of thiols (Huang et al. 2007) and biomolecules such as proteins (Zhou et al. 2009).

2.3.2 Uses in Medicine

AuNCs have uses in medicine due to their strong fluorescence. Since these particles can enter cells, they can be used for cellular labeling and enable scientists to track cells during experiments. They can also be used to sense the presence of other metals as demonstrated by Huang et al. (2007) who used the AuNCs to sense the presence of Hg(III). AuNCs are potential imaging agents as well, due to their ability to conjugate with other molecules, their biocompatibility and the ability of scientists to control their fluorescence (Chen et al. 2015).

2.3.3 Toxicity

AuNCs have been found to have very low *in vivo* toxicity. Toxicity is complicated since it will vary depending on cell type, nanocluster size, and ligands (Shang & Nienhaus 2012). However, AuNCs smaller than 5 nm can be metabolized by the kidneys and generally do not accumulate in other organs (Zhang et al. 2012). Multiple studies have found negligible toxicity in a variety of cell lines. Studies used mitochondrial damage to determine toxicity on

neuroblastoma cells, HeLa cells, and human endothelial cells. No damage was found (Shang & Nienhaus 2012).

2.4 Nanoparticles in Medicine

Nanoparticles are defined as particles 1 nm to 1,000 nm in diameter; molecules are generally excluded from this definition even when they fall in the size range. They have a wide variety of uses in medicine acting as targeted drug delivery systems. Nanoparticles can be synthesized to target biomolecules through affinity (Salata 2004). For example, the protein human serum albumin (HSA) complexed with a gold ion is used to target tumors since the tumor's vascular system will allow proteins to enter, but the drainage system will not permit the protein to exit the tumor. Nanoparticles provide a platform for the drug substance by giving the nanoparticle-drug substance complex the necessary properties to reach the target. The nanoparticles could be more soluble, more stable or less toxic than the drug alone (De Jong et al. 2008).

2.5 Human Serum Albumin

HSA (Figure 2) is a transport protein found in the bloodstream. HSA transports fatty acids, amino acids, steroids and metal ions from the circulatory system to the liver, intestines, kidneys and brain. These molecules are transported in one of the two hydrophobic pockets in HSA. Ions are transported through interactions with a free thiol on Cysteine 34 (He et al. 1992). HSA can transport pharmaceuticals as well. Drugs such as penicillin, sulfonamides, and benzodiazepines are carried through the body by HSA (Kratz 2008).

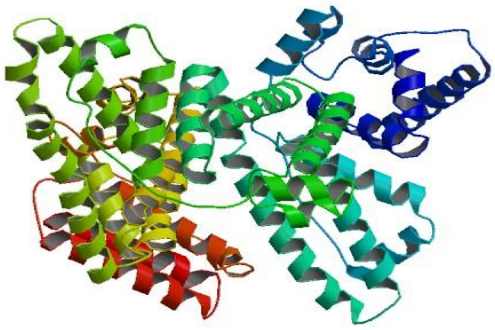

Figure 2: HSA structure (RCSB Protein Data Bank 2011)

HSA has been shown to accumulate in tumors by Matsumura and Maeda (1986). Tumors are highly permeable and large molecules like proteins are able to enter the tumor. However, they do not have a sufficient drainage system to allow large proteins to leave the tumor. This leads to a build up of HSA in the tumor, which can be exploited by imaging and drug delivery compounds (Merlot et al. 2014).

2.6 Arginylglycylaspartic Acid in Tumor Targeting

Arginylglycylaspartic acid (RGD) has been shown to be a tumor targeting compound by Haubner et al. (2001). It targets the $\alpha_v\beta_3$protein which is involved in angiogenesis, the formation of blood vessels to supply the tumor and the growth of a tumor. The RGD conjugated molecule showed a high affinity and selectivity for the tumor cells *in vivo* (Haubner et al. 2001).

2.7 Protein Based Imaging Compounds

2.7.1 Bovine Serum Albumin Gold Nanoparticles Biomineralization

Xie, Zheng and Ying (2008) created a one step biomineralization reaction to sequester gold ions in bovine serum albumin (BSA). Chloroauric acid ($HAuCl_4$) was added to a solution of BSA water allowing the BSA to sequester the gold ions. By increasing the pH using sodium

hydroxide (NaOH), the gold ions were reduced into gold nanoclusters consisting of 25 atoms. The fluorescence of the gold and BSA complex (Au@BSA) was red whereas the protein alone was pale blue (Figure 3).

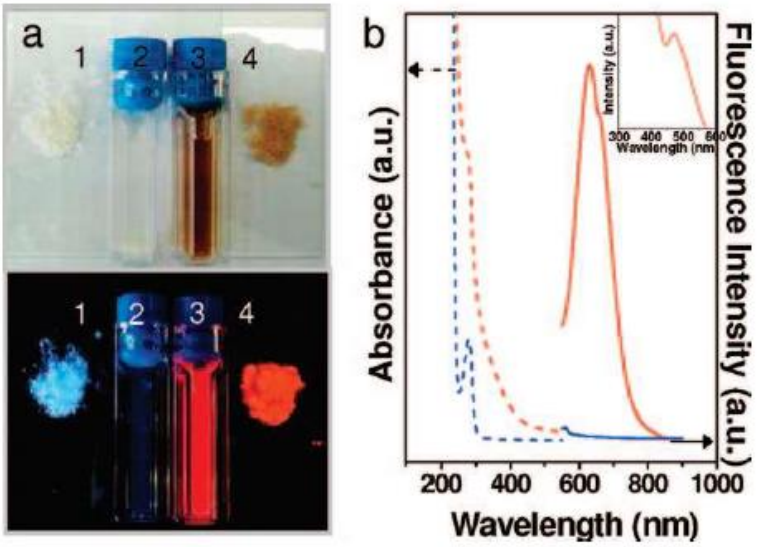

Figure 3: a. The color of the powdered BSA (1), aqueous BSA (2), aqueous Au@BSA (3), powdered Au@BSA under visible light (top) and UV light (bottom).b. Absorption (dashed) and emission at an excitation wavelength of 470 nm (solid) of BSA (blue) and Au@BSA (red) (Xie et al. 2008).

2.7.2 Bovine Serum Albumin Gold Nanoclusters Imaging

Wu et al. (2010) used a biomineralization reaction to form Au@BSA complexes using BSA and $HAuCl_4$. The Au@BSA complex was used in near infrared imaging; it was found that the complex accumulated in the tumor (Figure 4). The preferential accumulation in the tumor makes the Au@BSA a potential tumor targeting imaging compound.

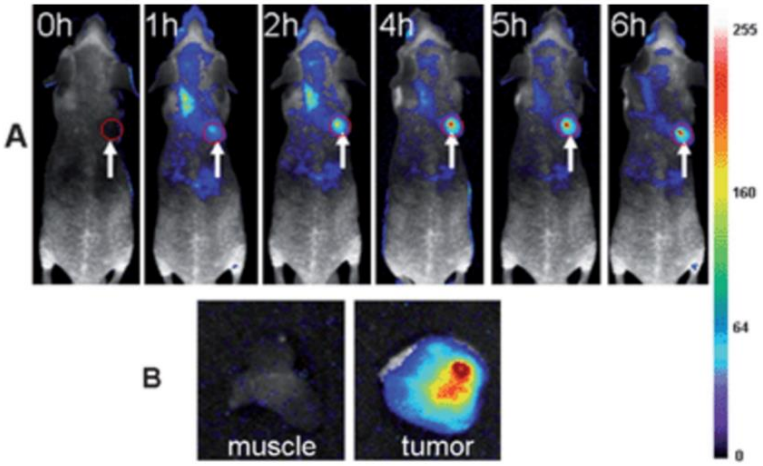

Figure 4: A) The strongest fluorescence signal was in the tumor circled in red over the six hours. B): *Ex vivo* imaging of the mouse's muscle and tumor (Wu et al. 2010).

The mouse's clearance of the Au@BSA compound was also monitored over a period of 24 hours. The compound remained in the body for a long enough time to allow for imaging to take place, but there were greatly decreased levels of fluorescence by 24 hours, see Figure 5.

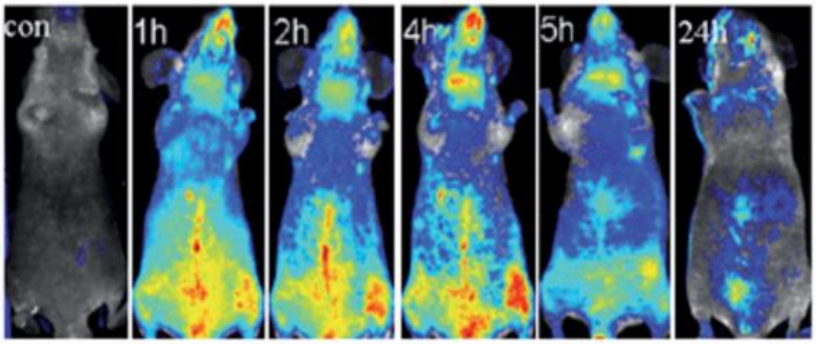

Figure 5: The fluorescence imaging of a mouse injected with Au@BSA over a period of 24 hours (Wu et al. 2010).

Wu et al. then monitored the mice for 4 weeks post injection to monitor for body weight and general behavior. The Au@BSA mice and the control mice showed the same body weight changes that the control exhibited, (Figure 6). The injected mice also showed no signs of distress or unusual behavior. This demonstrated that there was no toxicity of the Au@BSA complexes to the mice.

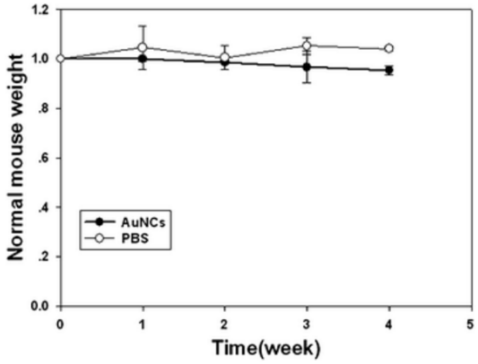

Figure 6: The change in body weight of the Au@BSA mice and the control mice over 4 weeks (Wu et al. 2010).

2.7.3 Human Serum Albumin Gold Nanoclusters

Zhao identified a biomineralization reaction that produced a red fluorescent Au@HSA compound. The E11 forms a gold nanocluster of around 25 gold ions. When tested using MRI in mice, it was found that Au@HSA appeared on the scans. It also accumulated in the tumor making this a promising tumor targeting contrast agent for use in MRI. The compound was eliminated via the kidneys and there was very little accumulation in other tissues.

3. Experimental

3.1 Preparation of Au@HSA and Au@BSA

Au@HSA was prepared by dissolving 240 mg of HSA in 8 mL of distilled water. Then, 4 mL of 10 mM $HAuCl_4$ was added dropwise and the resulting solution was stirred at 37°C. After 5 minutes, 800 μL of 1 M NaOH was added dropwise and then allowed to react overnight at 37°C while being stirred in the dark. Au@BSA was prepared identically except using 240 mg BSA in place of 240 mg HSA.

The Au@HSA and Au@BSA protein complexes were then purified by centrifuge filtration using a 30,000 D maximum particle size filter at 5000 rpm for 30 minutes. Phosphate-

buffered saline (PBS) was used to wash the compound three times. The compounds were stored at 4°C away from light.

3.2 Formation of Au@HSA

In order to form the Au@HSA RGD conjugated molecule (Au@HSA-RGD), 16 mg arginylglycylaspartic acid (RGD), 8 mg 4-dimethylaminopyridine (DMAP), and 6 mg 1-Ethyl-3-(3-dimethylaminopropyl)carbodiimide (EDC) were dissolved in 2 mL of distilled water and stirred for half an hour. In a separate vial, 3 mL of the purified Au@HSA was diluted with 2 mL of PBS. 1 mL of the RGD solution was added to diluted Au@HSA. The resulting solution was stirred for 24 hours at 4°C. The nanoparticles were then purified by centrifuge filtration as described above.

3.3 Analysis

The fluorescence emission and excitation spectra were obtained for Au@HSA, Au@BSA, and@BSA-RGD. 100μL of the purified and concentrated sample was added to 1mL of PBS. The emission and excitation spectra were obtained at 520 nm. The particle diameter of Au@HSA and Au@BSA was found through dynamic light scattering (DLS). The DLS sample was prepared from 20 μL of the purified, concentrated sample and 580 μL of PBS. The zeta potential of Au@HSA and Au@BSA were measured using a solution of 10 μL of the purified, concentrated sample in 1 mL of KCl.

4. Results and Discussions

4.1 Suitability as a Contrast Agent

4.1.1 Near Infrared Fluorescent Imaging

The Au@HSA and Au@HSA-RGD complexes have excitation peaks in the 810 nm range, 815 nm for the Au@HSA (Figure 7) and 810 nm for Au@HSA-RGD (Figure 8). These excitation peaks are in the NIR which is ideal for *in vivo* NIRFI since the tissue does not absorb light in this region. This is also similar to the emission found for Au@BSA, 815 nm (Figure 9) which was a viable *in vivo* contrast agent in Wu et al. (2010).

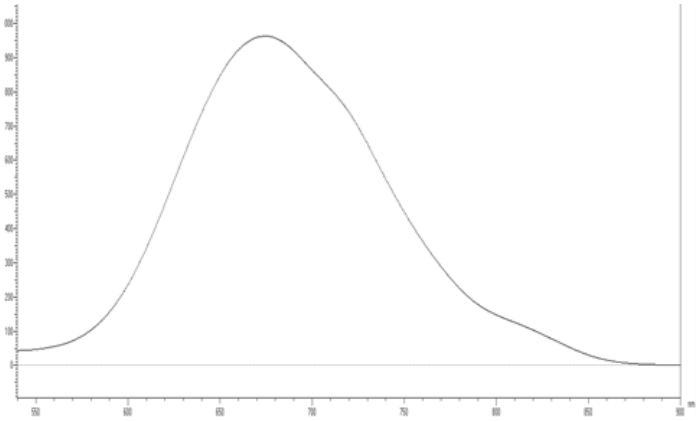

Figure 7: Emission Spectrum of Au@HSA at 520 nm with peaks at 675 nm and 815 nm

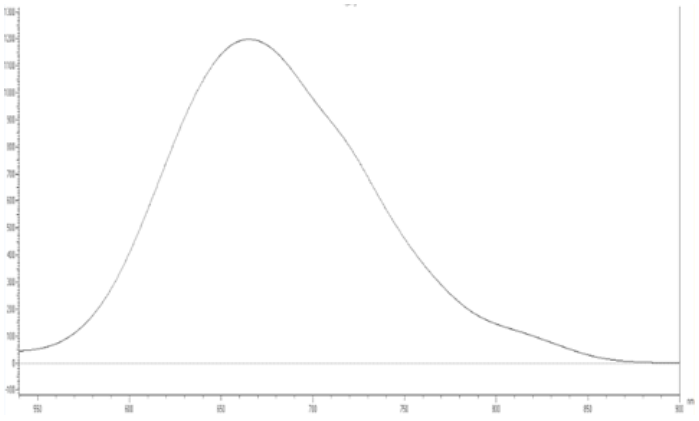

Figure 8: Emission Spectrum of Au@HSA-RGD at 520 nm with peaks at 665 nm and 810 nm

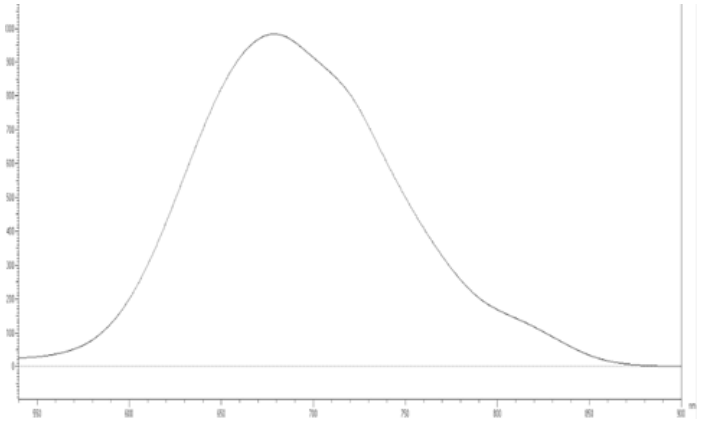

Figure 9: Emission Spectrum of Au@BSA at 520 nm with peaks at 687 nm and 810 nm

These complexes also exhibited fluorescence giving them the potential as an imaging probe. Au@HSA and Au@HSA-RGD had peaks at an excitation of 520 nm of 387 nm (Figure 10) and 388 nm (Figure 11) respectively. This fluorescence would be visible and allow for the visualization of the compound's accumulation in the body. These peaks show only a 10 nm shift in the fluorescence when conjugated with the RGD.

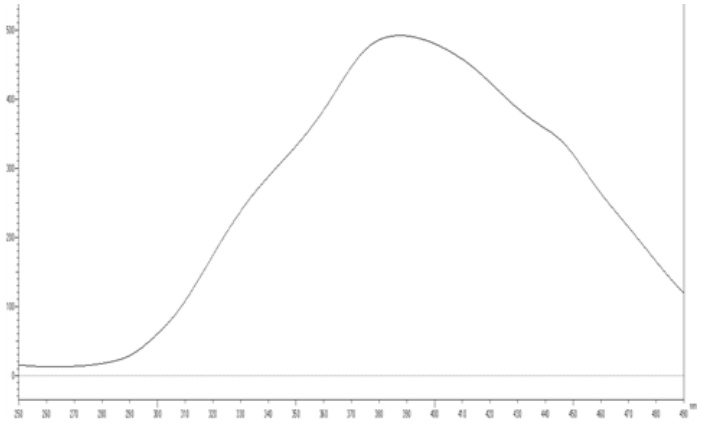

Figure 10: Excitation Spectrum of Au@HSA-RGD at 520 nm with a peak at 378 nm

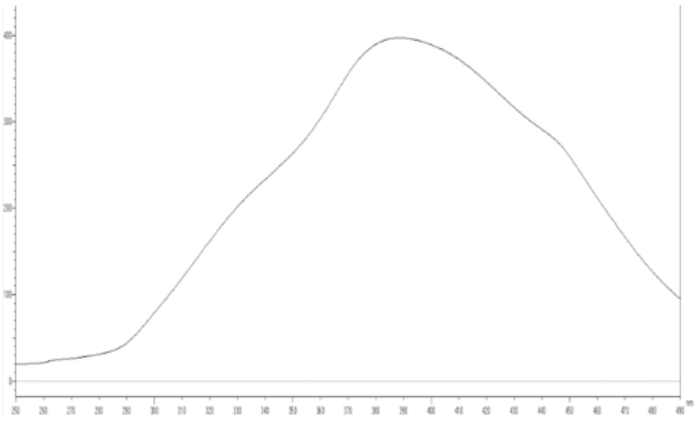

Figure 11: Excitation Spectrum of Au@HSA-RGD at 520 nm with a peak at 388 nm

The maxima for Au@HSA and Au@HSA-RDG are similar to the Au@BSA imaging compound researched by Wu et al. (2010). When the Au@BSA complex was synthesized in the lab, it was found to have a peak of 388 nm (Figure 12). Due to the similarity in emission wavelength the Au@HSA and Au@HSA-RGD should produce the same in the NIRFI results.

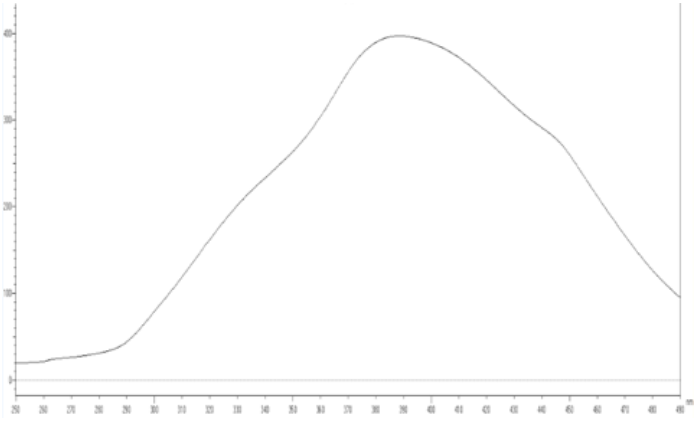

Figure 12: Excitation Spectrum of Au@HSA-RGD at 520 nm with a peak at 388 nm

4.1.2 Magnetic Resonance Imaging

The Au@HSA and Au@HSA-RGD complexes also show potential as MRI CAs. The HSA sequestered the gold ions which were then reduced to a neutral AuNC by the NaOH. The neutral atoms have three unpaired electrons which produce the magnetic moment needed for the

compound to show on the MRI readout. The MRI activity of the AuNCs has been confirmed by Chen et al. (2015).

4.2 Tumor Targeting Modification

The Au@HSA complex was successfully conjugated with the RGD. The shift in the excitation peak from 815 nm for the Au@HSA (Figure 7) to 810 nm for Au@HSA-RGD (Figure 8) shows that the molecular structure has been changed. Likewise, there was a shift in the emission peak from 387 nm (Figure 10) in Au@HSA to 388 nm (Figure 11) Au@HSA-RGD demonstrating that that there was conjugation between the Au@HSA and the RGD. The conjugation was also shown in the difference in particle size between the Au@HSA and the Au@HSA-RGD particles; it went from 7.836 nm to 12.310 nm after the conjugation (Table I).

Table I: Particle size		
Au@HSA	Au@BSA	Au@ HSA-RGD
7.836 nm	6.216 nm	12.31 nm

The research by Haubner et al. (2001) demonstrated that RGD conjugated molecule showed a high affinity for the tumor since it will bind to the $\alpha_v\beta_3$ protein. The conjugations of the Au@HSA complex with RGD should give the same tumor targeting ability.

4.3 Biocompatibility

Since HSA is a protein normally found in the bloodstream, it should be biocompatible. The Au@BSA compound was found to be biocompatible in Wu et al.'s (2010). HSA and BSA are analogous proteins with similar properties. Their Au complexes are similar in size, Au@HSA is 7.836 nm and Au@BSA is 6.216 nm (Table I). They also have comparable overall charges, Au@HSA is 17.0 mV and Au@BSA is 19.0 mV (Table II). These similarities imply that the proteins should have similar effects in the body.

Table II: Zeta Potential	
Au@HSA	Au@BSA
17.0 mV	19.0 mV

In Haubner et al. (2001) RGD conjugation was not found to change the toxicity. This means conjugating the Au@HSA complex with RGD should not change the biocompatibility.

5. Conclusion

The Au@HSA complex is a promising contrast agent for both optical imaging and MRI. Its optical properties make it a prime candidate since it will fluoresce from excitation by NIR which is suitable for *in vivo* imaging. The unpaired electrons in the AuNC make it MRI active enabling visualization of the tissue. The Au@HSA is formed by a simple one-pot synthesis with no harmful byproducts. Additionally the complex is biocompatible since it is based on a protein normally found in the human body. Au@HSA can also be used as a targeted compound through conjugation with RGD. The conjugated compound will preferentially accumulate in a tumor allowing for visualization of the tumor with MRI or NIRFI.

In the future, this research can be expanded upon given the promise of the Au@HSA. Additional research can focus on other applications of tumor targeting such as drug delivery. Using Au@HSA as a drug carrier would allow for the drug to be delivered directly to the tumor. Doctors could also monitor the location of the complex in the body and see where the drug is released. Experimentation with other metal ions would be possible using HSA as a base. Metals such as gadolinium ions could exhibit optical properties that would make it an even better imaging compound.

References

Darrah, T. H., Prutsman-Pfeiffer, J. J., Poreda, R. J., Ellen Campbell, M., Hauschka, P. V, & Hannigan, R. E. (2009). Incorporation of excess gadolinium into human bone from medical contrast agents. *Metallomics : integrated biometal science*, 1(6), 479–88.

Chen, L. Y., Wang, C. W., Yuan, Z., & Chang, H. T. (2015). Fluorescent gold nanoclusters: recent advances in sensing and imaging. *Anal. Chem*, *87*(1), 216-229.

De Jong, W. H., & Borm, P. J. (2008). Drug delivery and nanoparticles: applications and hazards. *International journal of nanomedicine*, 3(2), 133.

Frangioni, J. V. (2003). In vivo near-infrared fluorescence imaging. *Current opinion in chemical biology*, 7(5), 626-634.

Garland, M., Yim, J. J., & Bogyo, M. (2016). A bright future for precision medicine: advances in fluorescent chemical probe design and their clinical application. *Cell chemical biology*, 23(1), 122-136.

Haubner, R., Wester, H. J., Burkhart, F., Senekowitsch-Schmidtke, R., Weber, W., Goodman, S. L., ... & Schwaiger, M. (2001). Glycosylated RGD-containing peptides: tracer for tumor targeting and angiogenesis imaging with improved biokinetics. Journal of Nuclear Medicine, 42(2), 326-336.

He, X. M., & Carter, D. C. (1992). Atomic structure and chemistry of human serum albumin. *Nature*, 358(6383), 209-215.

Hornak, J.P. (2011-a). The Basics of MRI: Basic Imaging Techniques. Retrieved from: https://www.cis.rit.edu/htbooks/mri/inside.htm

Hornak, J.P. (2011-b). The Basics of MRI: Spin Physics. Retrieved from: https://www.cis.rit.edu/htbooks/mri/inside.htm.

Hornak, J.P. (2011-c). The Basics of MRI: Image Presentation. Retrieved from: https://www.cis.rit.edu/htbooks/mri/chap-10/chap-10.htm.

Hornak, J.P. (2011-d). The Basics of MRI: Introduction. Retrieved from: https://www.cis.rit.edu/htbooks/mri/inside.htm.

Huang, C. C., Yang, Z., Lee, K. H., & Chang, H. T. (2007). Synthesis of highly fluorescent gold nanoparticles for sensing mercury (II). *Angewandte Chemie*, 119(36), 6948-6952.

Kratz, F. (2008). Albumin as a drug carrier: design of prodrugs, drug conjugates and nanoparticles. *Journal of Controlled Release*, 132(3), 171-183.

Levy, L. M. (2007). Exceeding the limits of the normal blood-brain barrier: quo vadis gadolinium? AJNR. American journal of neuroradiology, 28(10), 1835–6.

Matsumura, Y., & Maeda, H. (1986). A new concept for macromolecular therapeutics in cancer chemotherapy: mechanism of tumoritropic accumulation of proteins and the antitumor agent smancs. *Cancer research*, 46(12 Part 1), 6387-6392.

Merlot, A. M., Kalinowski, D. S., & Richardson, D. R. (2014). Unraveling the mysteries of serum albumin—more than just a serum protein. *Frontiers in physiology*, 5, 299.

Pansare, V. J., Hejazi, S., Faenza, W. J., & Prud'homme, R. K. (2012). Review of long-wavelength optical and NIR imaging materials: contrast agents, fluorophores, and multifunctional nano carriers. *Chemistry of materials*, 24(5), 812-827.

Perazella, M. A. (2009). Current status of gadolinium toxicity in patients with kidney disease. *Clinical journal of the American Society of Nephrology : CJASN*, 4(2), 461–9.

Pirollo, K. F., Dagata, J., Wang, P., Freedman, M., Vladar, A., Fricke, S., ... & Chang, E. H. (2006). A tumor-targeted nanodelivery system to improve early MRI detection of cancer. *Molecular imaging*, 5(1), 7290-2006.

RCSB Protein Data Bank. (2011). Crystal Structure of Human Serum Albumin. Retrieved from:http://www.rcsb.org/pdb/explore.do?structureId=1ao6.

Rieter, W. J., Taylor, K. M., An, H., Lin, W., & Lin, W. (2006). Nanoscale metal-organic frameworks as potential multimodal contrast enhancing agents. *Journal of the American Chemical Society*, *128*(28), 9024-9025.

Salata, O. V. (2004). Applications of nanoparticles in biology and medicine. *Journal of nanobiotechnology*, 2(1), 1.

Shang, L., & Nienhaus, G. U. (2012). Gold nanoclusters as novel optical probes for in vitro and in vivo fluorescence imaging. *Biophysical Reviews*, 4(4), 313-322.

U.S. Food and Drug Administration. (2016-a). FDA Drug Safety Communication: FDA evaluating the risk of brain deposits with repeated use of gadolinium-based contrast agents for magnetic resonance imaging (MRI). Retrieved from: http://www.fda.gov/Drugs/DrugSafety/ucm455386.htm

U.S. Food and Drug Administration. (2016-b). Uses. Retrieved from: http://www.fda.gov/Radiation-EmittingProducts/RadiationEmittingProductsandProcedures/MedicalImaging/MRI/ucm482763.htm.

Wu, X., He, X., Wang, K., Xie, C., Zhou, B., & Qing, Z. (2010). Ultrasmall near-infrared gold nanoclusters for tumor fluorescence imaging in vivo. *Nanoscale*, 2(10), 2244-2249.

Xie, J., Zheng, Y., & Ying, J. Y. (2009). Protein-directed synthesis of highly fluorescent gold nanoclusters. *Journal of the American Chemical Society*, 131(3), 888-889.

Zhang, X. D., Wu, D., Shen, X., Liu, P. X., Fan, F. Y., & Fan, S. J. (2012). In vivo renal clearance, biodistribution, toxicity of gold nanoclusters. *Biomaterials*, 33(18), 4628-4638.

Zhou, R., Shi, M., Chen, X., Wang, M., & Chen, H. (2009). Atomically Monodispersed and Fluorescent Sub-Nanometer Gold Clusters Created by Biomolecule-Assisted Etching of Nanometer-Sized Gold Particles and Rods. *Chemistry–A European Journal*, *15*(19), 4944-4951.